

## Fatigue study on additional cutout between U shaped rib and floorbeam in orthotropic bridge deck

Xiaochen Ju\*, Zhibin Zeng, Xinxin Zhao and Xiaoguang Liu

China Academy of Railway Sciences, No.2 Daliushu Road, Haidian District, Beijing 100081, China

(Received November 18, 2017, Revised May 15, 2018, Accepted May 24, 2018)

**Abstract.** The field around additional cutout of the floor beam web in orthotropic bridge deck was subjected to high stress concentration, especially the weld toe between floor beam and U shaped rib and the free edge of the additional cutout. Based on different considerations, different geometrical parameters of additional cutout were proposed in European, American and Japanese specifications, and there remained remarkable differences among them. In this study, considering influence of out-of-plane deformation of floor beam web and U shaped rib, parameter analysis for additional cutout under typical load cases was performed by fine finite element method. The influence of additional cutout shape and height to the stress distribution around the additional cutout were investigated and analyzed. Meanwhile, the static and fatigue test on this structure details was carried out. The stress distribution was consistent with the finite element analysis results. The fatigue property for additional cutout height of 95mm was slightly better than that of 61.5 mm.

**Keywords:** fatigue property; additional cutout; out-of-plane deformation; orthotropic bridge deck; parameter analysis

### 1. Introduction

The orthotropic bridge deck has been widely used due to lighter weight and shorter construction time (Wolchuk and Baker 2004, Sim and Uang 2012). It was composed of longitudinal and transverse members which were welded into a whole to work together, as shown in Fig. 1. The orthotropic bridge deck had a large ultimate bearing capacity under the uniform load or concentrated load, and it was suitable for both vertical and horizontal moving loads. However, bending deformation was produced in the longitudinal and transverse members under wheel loads, which caused serious stress concentration in welding connection field.

Fatigue problem was often produced in bridge engineering (Deshmukh *et al.* 2014, Hong *et al.* 2014, Fettahoglu 2015, Xin *et al.* 2015, Kainuma *et al.* 2015, Ataei *et al.* 2016, Nagy *et al.* 2016). Until now, many types of fatigue cracks had been found at the welding connection field in orthotropic bridge deck (Miki 2006, Xiao *et al.* 2008, Ya 2011, Sonsino *et al.* 2012, Huang *et al.* 2016), as shown in Fig. 1. Among the fatigue cracks, there were three types of cracks found around additional cutout of the floor beam web: crack originating from the free edge of the additional cutout, crack originating from weld toe and propagating along U shaped rib web and crack originating from weld toe and propagating along floor beam web.

According to statistics on fatigue crack in orthotropic bridge deck in Hanshin Expressway and Shuto Expressway from Japan Steel Structure Committee in 2007, the fatigue

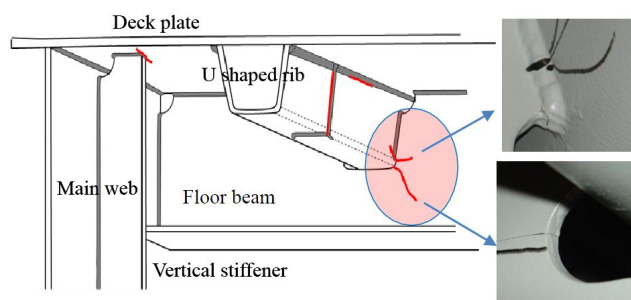


Fig. 1 Typical cracks in orthotropic bridge deck

cracks around additional cutout of the floor beam web accounted for more than half of total crack in orthotropic bridge deck. The force state around additional cutout was relatively complicated (Corte and Bogaert 2007), which was affected by the geometry of the additional cutout. In order to make it more clear, some researchers (Wolchuk and Baker 2004, Dexter and Fisher 1995, Corte and Bogaert 2007, Wang *et al.* 2015) calculated and measured stress distribution around the cutout. Based on Vierendeel truss analogy, a calculation model of stress distribution around additional cutout was proposed by Haibach (Haibach and Plásil 1983) and developed by Corte and Bogaert (2007).

In this study, considering the out-of-plane bending deformation of floor beam web and U shaped rib, parameter analysis on stress state around additional cutout was performed employing fine finite solid element model, and the weld was established in the model, which made the stress state in FEM more close to that in real bridge. Based on the analysis, the reasonable geometry of additional cutout was proposed. Besides, a new fatigue test method was invented and adopted; the fatigue property of this

\*Corresponding author, Ph.D., Professor,  
E-mail: [juxc2008@163.com](mailto:juxc2008@163.com)

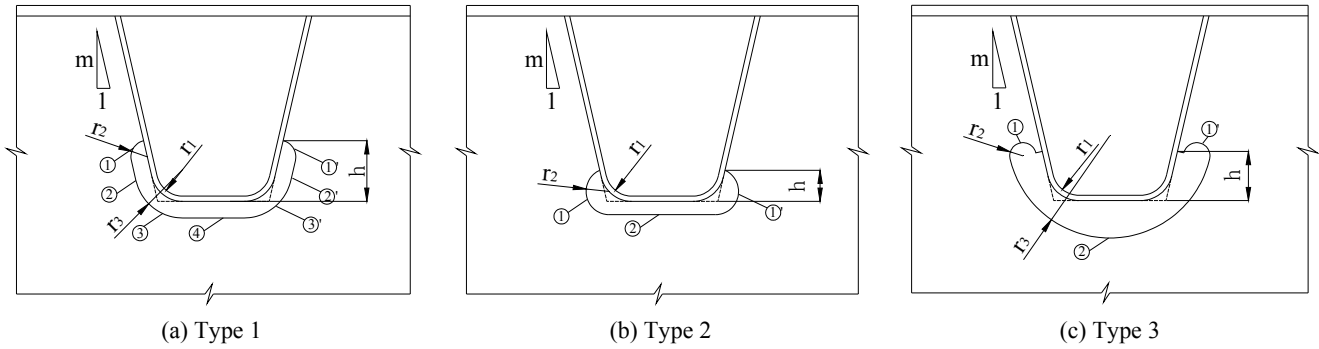


Fig. 2 Typical additional cutout

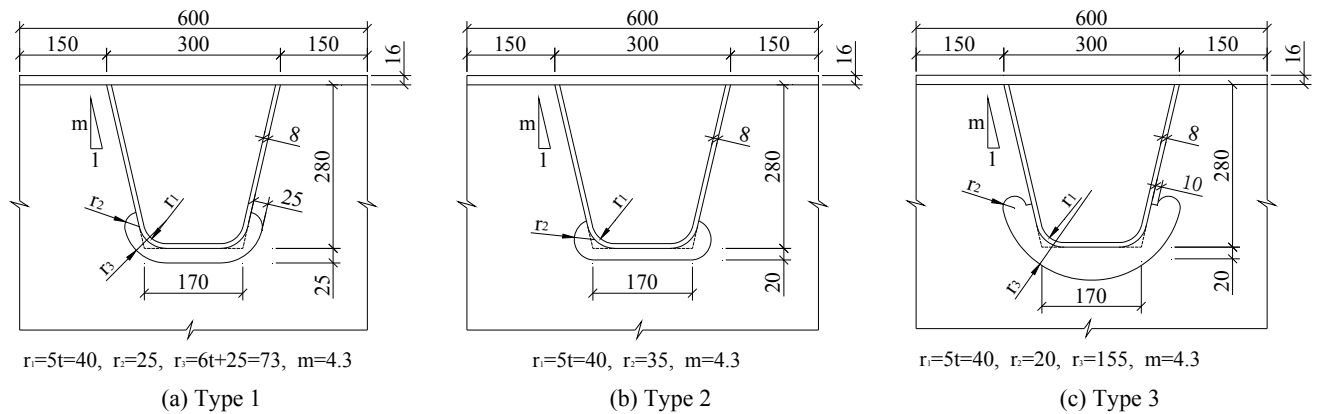


Fig. 3 Geometrical dimensions of additional cutout

structure detail with different cutouts height was investigated.

## 2. Typical additional cutout

The typical additional cutout adopted in real bridge were showed in Fig. 2. The cutout profile in Fig. 2(a) was composed of 7 sections of the line. Section ①, ①', ③ and ③' were circular arc, and section ②, ②' and ④ were straight line. In some additional cutout adopted in bridge, 7 sections were transferred into 5 sections, and section ② and ②' were disappeared in it. The additional cutout in Fig. 2(a) was most widely used. European (Eurocode 3 2009), American (AASHTO 2012) and Japanese (JRA 2002) bridge design specifications provided different parameter design requirements for it. The distance of 20 mm and 25 mm between the lower flange of U shaped rib and section ④ of additional cutout was adopted in JRA and Eurocode3, respectively. AASHTO required that the height of additional cutout ( $h$  was showed in Fig. 2) should be not less than one third of the height of height of U shaped rib.

The additional cutout in Fig. 2(b) was made up of 3 sections, section ① and ①' were arc and section ② was straight line. It was adopted in some Chinese highway steel bridges. The cutout profile showed in Fig. 2(c) was mainly composed of 3 section of arc, which was recommended to use in railway orthotropic bridge deck in Eurocode 3.

## 3. Finite element analysis

### 3.1 Geometrical dimensions of additional cutout

The basic model has a rib spacing of 600 mm and a rib height of 280 mm. The ribs are closed U shaped ribs (upper width = 300 mm / lower width = 170 mm), the thickness of ribs is 8mm, and the radius of transitions is 5 t ( $t$  is the thickness of rib web). Three types of additional cutout were selected to analyze. The geometrical dimensions of the additional cutouts were showed in Fig. 3. In addition, parameter analysis for the height of Type 1 additional cutout was performed.

### 3.2 Finite element model information

A section model of steel box girder steel bridge deck were selected as computing object, whose local rigidity under wheel load was close to that of real bridge deck. Six U shaped ribs and four floor beams were included in the model. The geometrical dimensions of the model were showed in Fig. 4.

The fine finite element models with different additional cutouts were established employing software ABAQUS. Three-dimensional eight-node elements were adopted. In order to eliminate the influence on stress results from element size to ensure the comparability of stress results from different models, the element sizes of the field around additional cutouts for all types of cutouts were controlled in

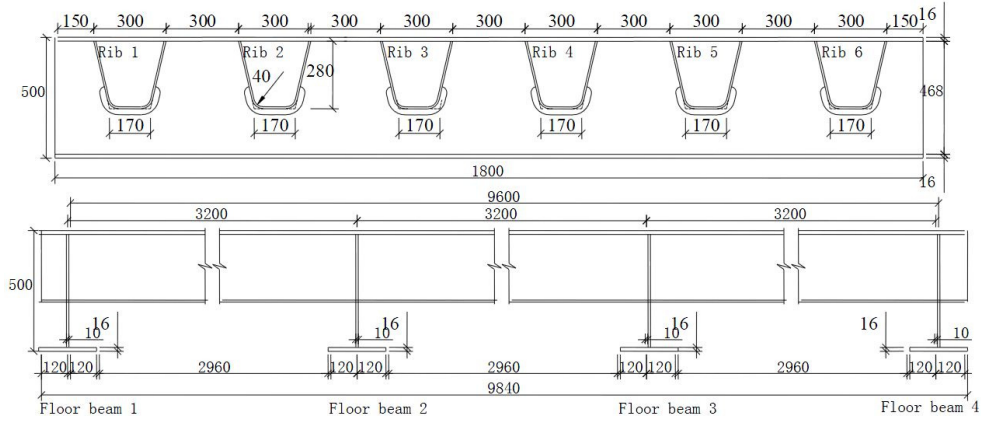


Fig. 4 Section model

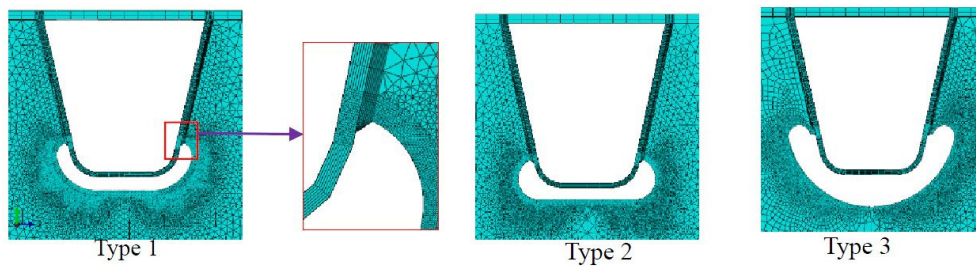


Fig. 5 Fine finite element mesh

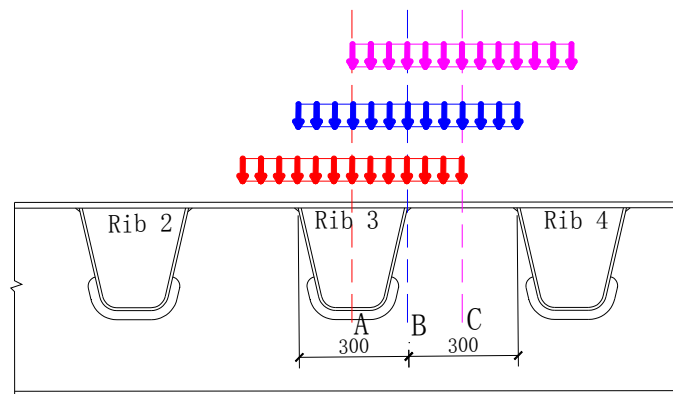


Fig. 6 Load cases

2 mm × 2 mm × 2 mm, as shown in Fig. 5. The floor beam web in steel box girder of suspension bridge produced very small vertical displacement under wheel load, therefore, the four lower flanges of the floor beams of the model were constrained in vertical direction.

### 3.3 Load cases

According to “General Specifications for Design of Highway Bridges and Culverts (JTG D60-2004)”, standard values of rear axle vehicle load was 140 kN, the loading action area was 200 mm × 600 mm. The uniform pressure on action area was 1166.667 kN/m<sup>2</sup>. In this analysis, three typical transverse load positions were selected: right above the U shaped rib (Line A), above one side of the U shaped

rib (Line B) and above the adjacent two U-shaped ribs (Line C). From one floor beam to mid-span of two floor beams, nine load positions (200 mm per interval) in longitudinal direction were selected in Fig. 6. Totally, there were 27 loading positions in the analysis model.

### 4. Analysis results and discussion

Three typical types of fatigue cracks around additional cutout were showed in Fig. 7: crack originating from the free edge (Point ①) of the additional cutout, crack originating from weld toe (Point ③) and propagating along U shaped rib web and crack originating from weld toe (Point ②) and propagating along floor beam web. Through

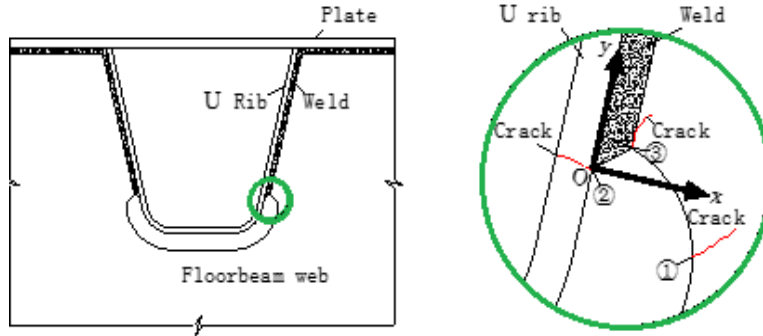


Fig. 7 Crack around additional cutout of floor beam web

Table 1 Max-principal stress distribution near weld toe (MPa)

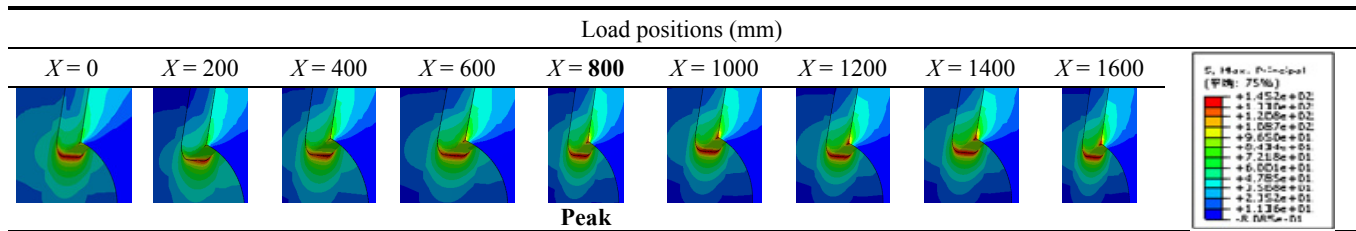
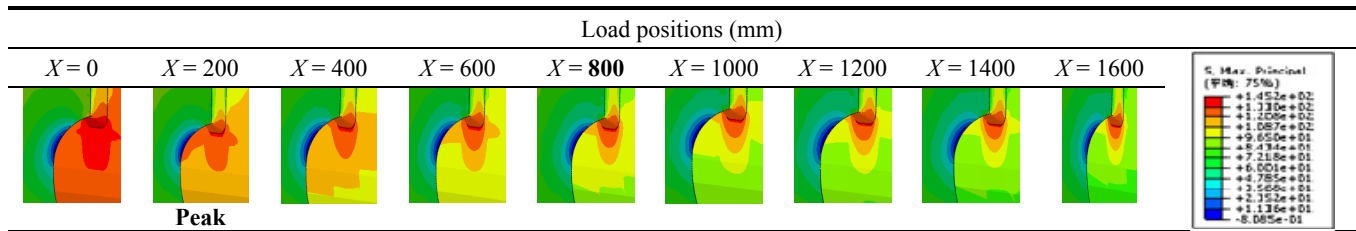


Table 2 Min-principal stress distribution around additional cutout edge (MPa)



a pre-computation, it was found that there was obvious stress concentration in the three points. The point ② and point ③ was mainly in tensile state, and the point ① was in pressure state. Therefore, the minimum principal stress at point ① and the maximum principal stress at point ② were extracted and analyzed.

#### 4.1 Stress distribution around additional cutout

Take stress state around additional cutout under line C for instance. Table 1 showed the max-principal stress distribution around weld toe (Point ② and Point ③) and the corresponding peak value position. The max-principal stress distribution change obviously with the movement of load from floor beam to mid-span of two floor beams, and the stress concentration behavior developed from just existing at point ② singly to coexisting at point ② and point ③. The maximum values increased first and then decreased, and the peak value of max-principal stress produced when load center was at  $X = 800$  mm. Table 2 showed the min-principal stress distribution around cutout edge (Point ①) and corresponding peak value position. There was obvious stress concentration at the cutout edge. The stress concentration almost kept at same position in all

loading cases, and the peak value of min-principal stress occurred when load center at  $X = 200$  mm.

From the stress distribution results shown in Table 1, it was found that most serious tensile stress concentration

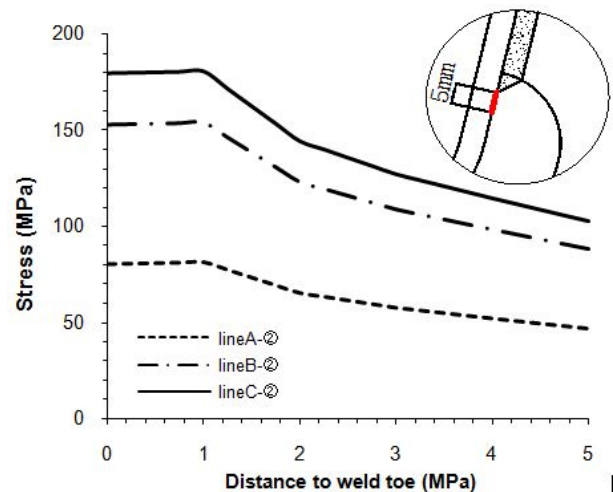


Fig. 8 Stress variation in the range within 5 mm from weld toe

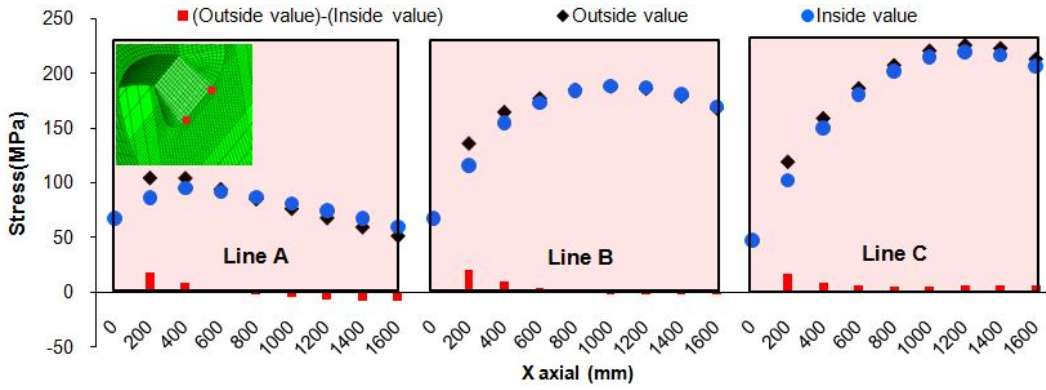


Fig. 9 Difference between the inside and outside values at Point ②

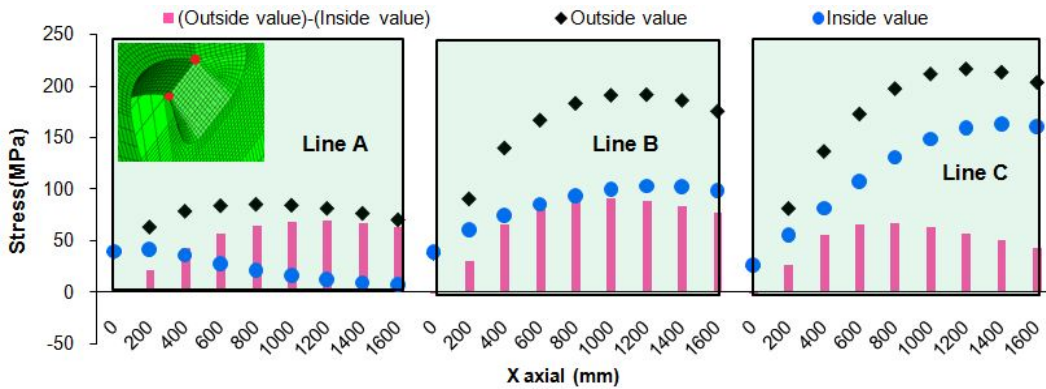
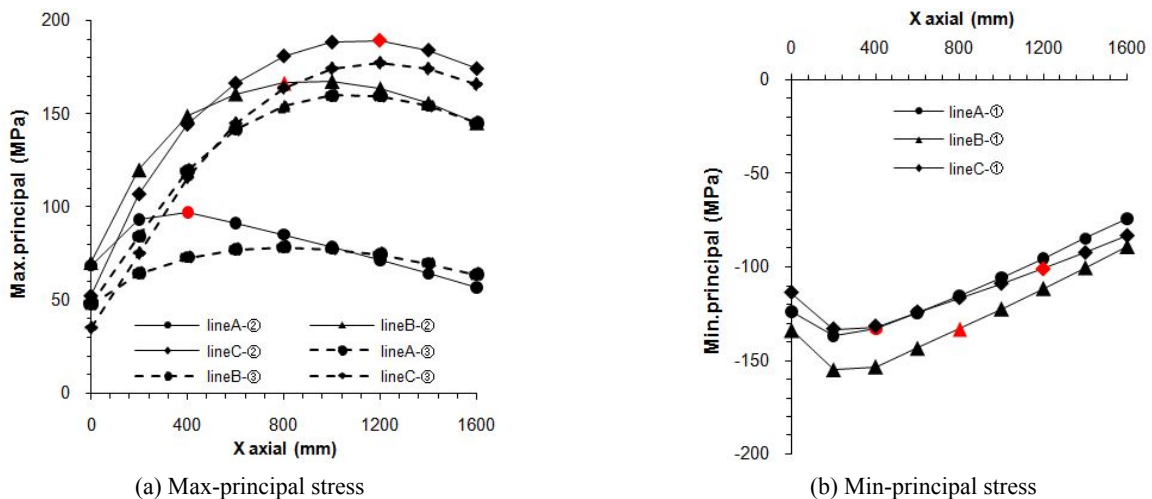


Fig. 10 Difference between the inside and outside values at Point ③

behaved in floor beam web near weld toe, which implied that fatigue crack was prone to happen there. Fig. 8 showed the y direction stress (in local coordinate in Fig. 7) variation in the range within 5 mm from weld toe in floor beam web at  $X = 800$ . The stress in the range with 1 mm from weld toe kept nearly same, and then decreased away from weld toe.

Fig. 9 showed the difference between the inside and outside values at Point ②. As a whole, the difference between them were relatively small, which meant that the

stress state Point ② was slightly affected by the out-of-plan deformation of the floor beam and U shaped rib. Under load at line B and Line C, outside values were a little larger than inside values. Under load at line A, outside values were larger than inside values when load closed to floor beam, however, it was opposite when load approaching mid-span of two floor beams. Fig. 10 showed the difference between the inside and outside values at Point ③. Outside values were obviously larger than inside values, which was mainly



(a) Max-principal stress

(b) Min-principal stress

Fig. 11 Stress variation with load movement

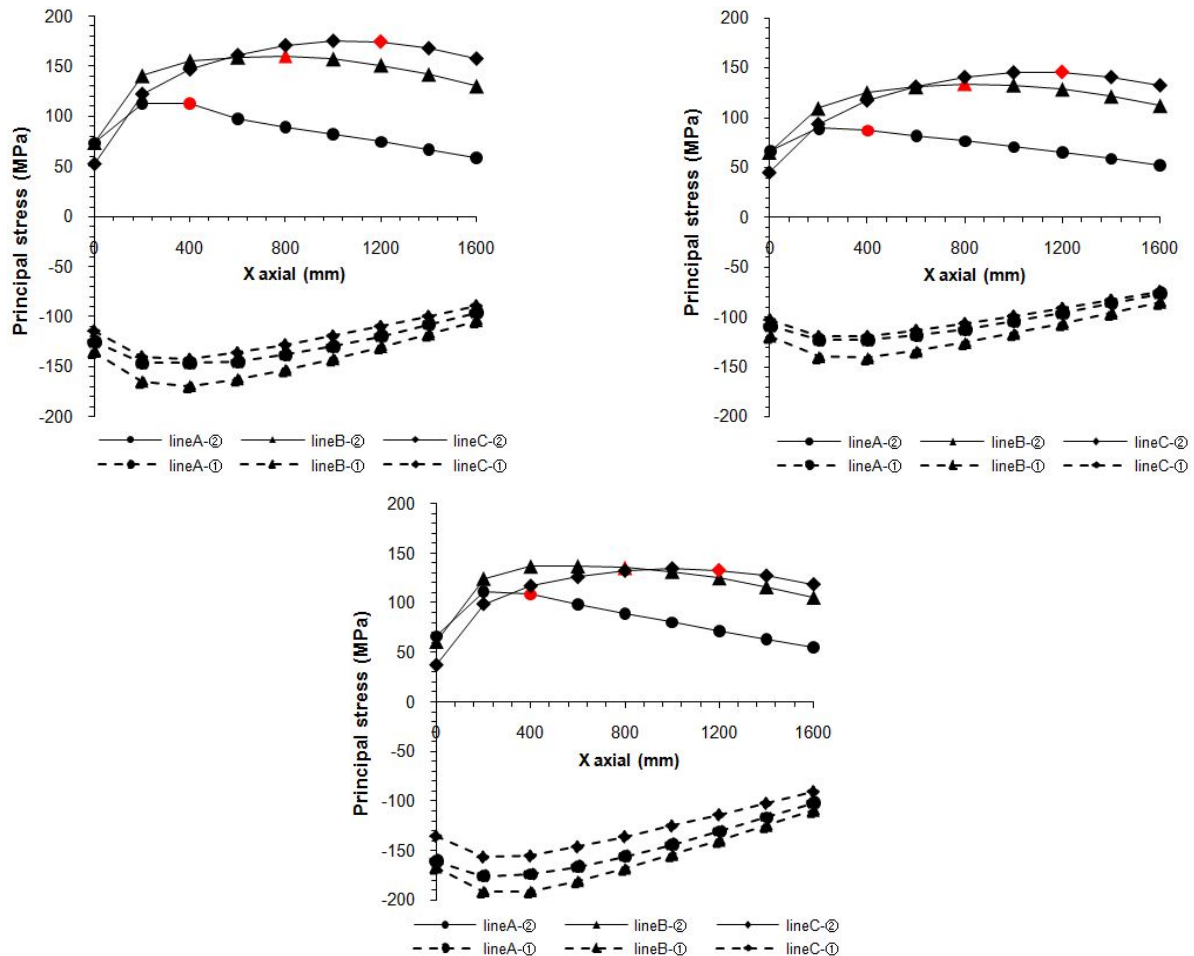


Fig. 12 Principal stress variation for three types of additional cutout

resulted from the out-of-plan deformation of the floor beam. The maximal difference produced in load at  $X = 600\sim 1000$  mm.

Fig. 11 showed the stress variation with load movement. Overall, max-principal stress at point ② behaved larger than that at point ③ as shown in Fig. 11(a). Among the three transverse load positions, load acting above the adjacent two U-shaped ribs (Line C) led to maximal max-principal stress, which distanced about 800 mm from floor beam in longitudinal direction. In Fig. 11(b), it could be found that the min-principal stress performance was adverse when load at Line B, and the minimal min-principal stress occurred when load distanced about 200 mm from floor beam.

## 4.2 Parameter analysis on stress state

### 4.2.1 Influence of additional cutout shape

Fig. 12 showed the principal stress variation for three types of additional cutout. From the analysis in Section 3.1, it was confirmed that max-principal stress at point ② was larger than that at point ③. According to the 2 mm hot stress method in IIW, the hot stress at point ② larger than that at point ③, too. Therefore, the max-principal stress at point ② was mainly extracted and discussed. The

principal stress for three different types of additional cutout behaved similar change regulation with load movement in transverse and longitudinal directions. Fig. 13(a) showed the max-principal stress of three types of additional cutout, and the relationship of the max-principal stress: Type 1 > Type 2 > Type 3; as shown in Fig. 13(b), the relationship of min-principal stress: Type 3 > Type 1 > Type 2. From the analysis result, it could be inferred that fatigue crack initiating at weld toe was prone to produce in Type 1 additional cutout, and fatigue crack initiating at cutout edge was easy to occur in Type 3 additional cutout, which coincided with the actual situation of fatigue crack statistics in orthotropic steel bridge deck. Although the min-principal stress for Type 3 additional cutout was largest, it did not mean that the edge of cutout was in fully compressed state in all load cases, and it was confirmed that there existed most serious stress concentration.

### 4.2.2 Influence of additional cutout height

The additional cutout height ( $h$ ) was an important influencing factor to stress state around additional cutout. JRA didn't make detailed provision for additional cutout height, but the value was generally less than 65 mm. AASHTO described clearly that the height of additional cutout should be equal or greater than one third of the height of U shaped rib, which was more than 90 mm. In this

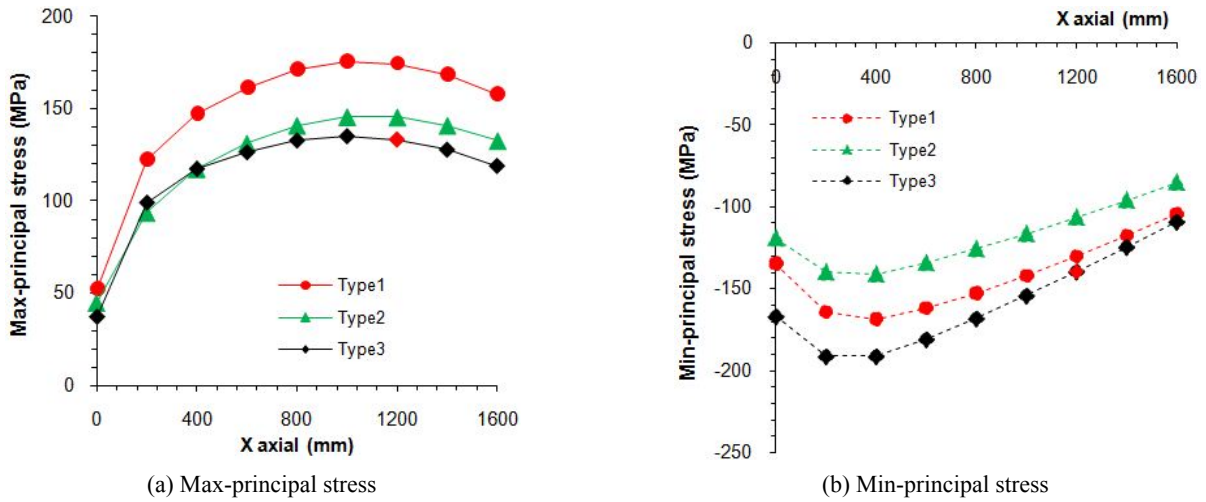


Fig. 13 Principal stress difference for three types of additional cutout

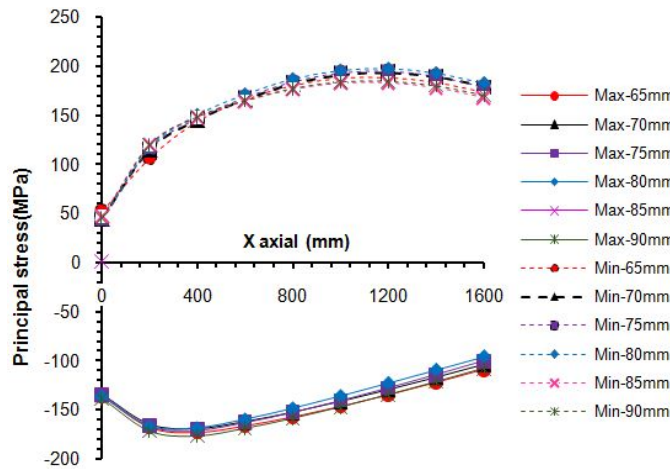


Fig. 14 Principal stress for different additional cutout height

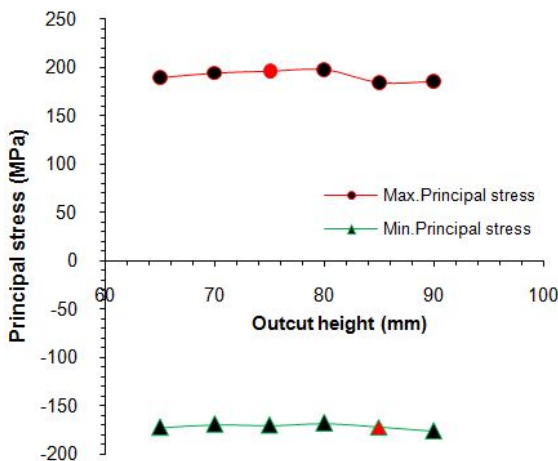


Fig. 15 Peak values change of principal stress for different additional cutout height

under load at Line C and min-principal stress at point ③ under load at Line B for different additional cutout height. The stress change regulation for different additional cutout height stayed the same. As shown in Fig. 15, the peak values of max-principal stress were relatively small when the additional cutout height were bigger (90 mm) or smaller (65 mm); the peak values of min-principal were nearly same for different additional cutout height. From the result above, it could infer that the additional cutout with relatively big or small height showed better fatigue property, which was consistent with JRA and AASHTO design requirements.

## 5. Fatigue test

### 5.1 Introduction of test

The static and fatigue test for two extreme additional cutout height ( $h$ ) of 61.5 mm (Specimen Number: LT1-1~LT1-6) and 95 mm (Specimen Number: LT2-1~LT2-6) was carried out, the test specimen consisted of two U shaped rib and one floor beam and the dimensions was

analysis, the finite element models with  $h = 65$  mm, 70 mm, 75 mm, 80 mm, 85 mm, 90 mm were selected to analyze. Fig. 14 showed max-principal stress at point ②



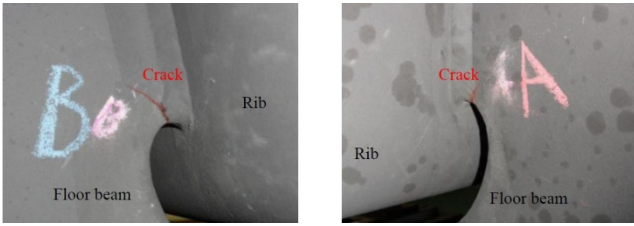


Fig. 19 Crack initiating from point ③ and propagating in floor beam web

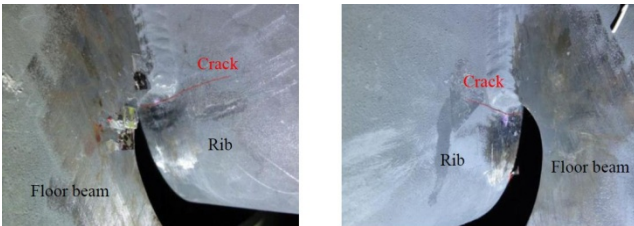


Fig. 20 Crack initiating from point ② and propagating in U shaped rib

from the weld between U shaped rib wall and floor beam web, which mainly contained two type of cracks. Type 1 crack initiated from point ② and propagated in U shaped rib to an angle of 45° with weld bead, and Type 2 initiated from point ③ and propagated in floor beam web along longitudinal direction. There was no crack initiating from cutout edge (point ①). The crack found in the test was showed in Figs. 19 and 20. It could be found that all crack originated from the field with serious stress concentration, which bought into correspondence with finite element analysis and static test.

Actually, the fatigue strength of this structure detail is difficult to describe by S-N fatigue curve. In the static test, it had been found that the force state around additional

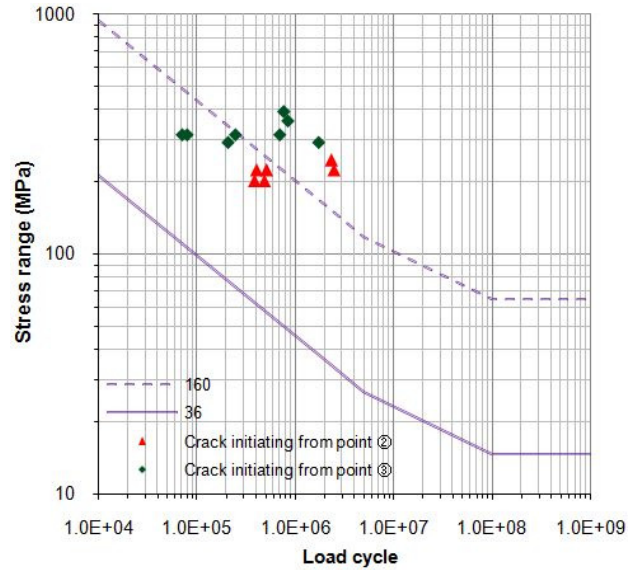


Fig. 22 Relationship between stress range and load cycle for difference crack types

cutout was quite complicated, and the nominal stress near the weld toe is almost impossible to obtain accurately. The hot spot stress which was 2 mm apart from the weld toe was employed by FE calculation. As shown in Fig. 21, the relationship between hot spot stress at weld toe and load cycle was provided, meanwhile, as a reference, the Euro code fatigue S-N curves for fatigue strength of 36 MPa and 160 MPa was charted. As a whole, the fatigue property for additional cutout height of 95 mm was slightly better than that of 61.55 mm. The curve gradient (m) for additional cutout height of 95 mm was higher than that for additional cutout height of 61.5 mm. Fig. 22 showed the relationship between stress range and load cycle for two type of cracks, it can be found that the fatigue strength at point ③ was higher than that at point ②.

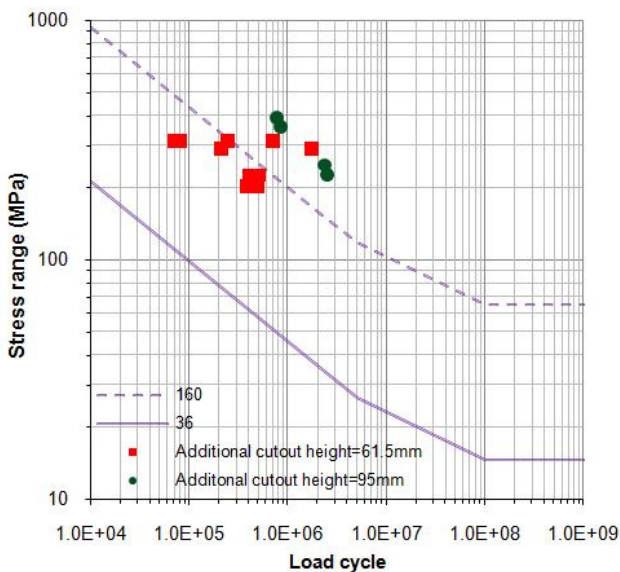
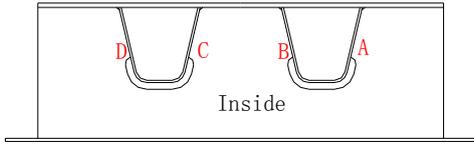


Fig. 21 Relationship between stress range and load cycle for difference additional cutout height

## 6. Conclusions

Considering weld size, the finite element analysis was carried out. The influence of additional cutout shape and height to the force state around additional cutout were investigated under different load cases in the analysis. There were serious stress concentration around additional cutout, and the most serious stress concentration point was about 1 mm far from weld toe. Among the three typical transverse load position, min-principal stress performance was adverse when load above one side of the U shaped rib (Line B), and the minimal min-principal stress occurred when load center distanced about 200 mm from floor beam in longitudinal direction. Load acting above the adjacent two U-shaped ribs (Line C) led to maximal max-principal stress, which distanced about 1000 mm from floor beam in longitudinal direction. In the three types of additional cutout, fatigue crack initiating at weld toe was prone to produce in Type 1 cutout, and fatigue crack initiating at cutout edge was easy to occur in Type 3 cutout, which coincided with the actual situation of fatigue crack statistics in orthotropic steel

Table 2 Fatigue test results



Specimen number	Load range ( kN )	Crack position	Load cycle	
h = 61.5 mm	LT1-1	B, floor beam web, inside	208110	
		C, floor beam web, inside	1738967	
	LT1-2	A, floor beam web, inside	70873	
		B, floor beam web, inside	79592	
		C, floor beam web, inside	247297	
	LT1-3	150	D, floor beam web, outside	699923
B,U shaped rib wall, outside			402116	
90		C,U shaped rib wall, inside	509071	
		No crack	2000000	
h = 95 mm	LT1-4	110	No crack	2000000
	LT1-6	135	B,U shaped rib wall, inside	383903
			C,U shaped rib wall, outside	484961
	LT2-1	125	No crack	2000000
	LT2-2	150	B,U shaped rib wall	2511271
	LT2-3	160	C, floor beam web, inside	845200
LT2-4	175	No crack	2000000	
LT2-5	165	C, U shaped rib wall	2360300	
LT2-6	175	C, floor beam web, inside	766359	

bridge deck. The additional cutout with relatively big or small height had better fatigue property, which was consistent with design specifications.

The static and fatigue test for additional cutout height of 61.5 mm and 95 mm was carried out. In the test, the floor beam web was subjected to in-plane and out of plane deformation, which approached to the force state of actual bridge. From the static test, it could be found that Point ① and point ③ was in larger stress state when additional cutout height of 95 mm, but the point ② existed larger stress when additional cutout height of 61.5 mm. From the fatigue test, it showed that it mainly produced two type of cracks: crack initiating from point ② and propagating in U shaped rib to an angle of 45° with weld bead, and crack initiating from point ③ and propagating in floor beam web along longitudinal direction. The fatigue property for additional cutout height of 95 mm was slightly better than that of 61.5 mm.

## References

- American Association of State Highway and Transportation Officials (2012), *LRFD Bridge Design Specifications*, (6th Ed.), Washington, DC, USA.
- Ataei, S., Tajalli, M. and Miri, A. (2016), "Assessment of load carrying capacity and fatigue life expectancy of a monumental Masonry Arch Bridge by field load testing: A case study of veresk", *Struct. Eng. Mech., Int. J.*, **59**(4), 703-718.
- Choi, J.H. and Kim, D.H. (2009), "Stress characteristics and fatigue crack behaviour of the longitudinal rib-to-cross beamjoints in an orthotropic steel deck", *Adv. Struct. Eng.*, **11**(2), 189-198.
- Corte, W.D. and Bogaert, P.V. (2007), "Improvements to the analysis of floor beams with additional web cutouts for orthotropic plated decks with closed continuous ribs", *Steel Comp. Struct., Int. J.*, **7**(1), 1-18.
- Dexter, R. and Fisher, J. (1995), "Fatigue cracking of orthotropic steel decks", *Proceedings of the Nordic Steel Conference 1995*, Malmö, Sweden, June.
- Deshmukh, A.R., Venkatachalam, G., Divekar, H. and Saraf, M.R. (2014), "Effect of weld penetration on fatigue life", *Procedia Eng.*, **97**, 783-789.
- Eurocode 3 (2009), Design of steel structures; DRAFT prEN.
- Fettahoglu, A. (2015), "Effect of cross-beam on stresses revealed in orthotropic steel bridges", *Steel Comp. Struct., Int. J.*, **18**(1), 149-163.
- Haibach, E. and Pläsil, I. (1983), "Untersuchungen zur Betriebsfestigkeit von Stahlleichtfahrbahnen mit Trapezhohlsteifen im Eisenbahnbrückenbau", *Der Stahlbau*, **83**(9), 269-274.
- Hong, S.N., Park, J.G., Park, S.K. and Choi, J.W. (2014), "Analysis of the Fatigue Stress on Welded Joints of the U-rib in an Orthotropic Steel Deck", *Proceedings of the 11th International Fatigue Congress on Advanced Materials Research*, Melbourne, Australia, March, pp. 1694-1698.
- Huang, T.L., Zhou, H., Chen, H.P. and Ren, W.X. (2016), "Stochastic modelling and optimum inspection and maintenance strategy for fatigue affected steel bridge members", *Smart*

- Struct. Syst., Int. J.*, **18**(3), 569-584.
- Japan Road Association (2002), Fatigue design guidelines for steel highway bridges, Tokyo.
- Kainuma, S., Jeong, Y.S., Ahn, J.H., Yamagami, T. and Tsukamoto, S. (2015), "Behavior and stress of orthotropic deck with bulb rib by surface corrosion", *J. Constr. Steel Res.*, **113**, 135-145.
- Leendertz, J.S. (2008), "Fatigue behaviour of closed stiffener to crossbeam connections in orthotropic steel bridge decks", *Civil Eng. Geosci.*, **40**(3), 217-259.
- Lu, P.M., Wang, L.F., Li, D.T., Lei, J. and Zhang, X.L. (2015), "Fatigue performance on the rounded welding region of U-rib and diaphragm of orthotropic steel bridge deck", *J. Chang'an Univ.*, **6**, 63-70.
- Miki, C. (2006), "Fatigue damage in orthotropic steel bridge deck and retrofit works", *J. Steel Struct.*, **6**, 255-267.
- Nagy, W., Schotte, K., Van Bogaert, P. and De Backer, H. (2016), "Fatigue strength application of fracture mechanics to orthotropic steel decks", *Adv. Struct. Eng.*, **19**(11), 1696-1709.
- Sim, H.B. and Uang, C.M. (2012), "Stress analyses and parametric study on full-scale fatigue tests of rib-to-deck welded joints in steel orthotropic decks", *J. Bridge Eng.*, **17**(5), 765-773.
- Sonsino, C.M., Fricke, W., De Bruyne, F., Hoppe, A., Ahmadi, A. and Zhang, G. (2012), "Notch stress concepts for the fatigue assessment of welded joints—Background and applications", *Int. J. Fatigue*, **34**(1), 2-16.
- Wang, B., Lu, P. and Shao, Y. (2015), "Research on rib-to-diaphragm welded connection by means of hot spot stress approach", *Steel Comp. Struct., Int. J.*, **18**(1), 135-148.
- Wolchuk, R. and Baker, G. (2004), "Orthotropic deck bridges", *Proceedings of Orthotropic Bridge Conference*, Reston, VA, USA, August.
- Xiao, Z.G., Yamada, K., Ya, S. and Zhao, X.L. (2008), "Stress analysis and fatigue evaluation of rib-to-deck joints in steel orthotropic decks", *Int. J. Fatigue*, **30**(8), 1387-1397.
- Xin, H., Liu, Y., He, J., Fan, H. and Zhang, Y. (2015), "Fatigue behavior of hybrid GFRP-concrete bridge decks under sagging moment", *Steel Compos. Struct., Int. J.*, **18**(4), 925-946.
- Ya, S. (2011), "Fatigue evaluation of rib-to-deck welded joints of orthotropic steel bridge deck", *J. Bridge Eng.*, **16**(4), 492-499.